A 3D model of the thorax for seismocardiography

Alexandre Laurin[1], Sébastien Imperiale[2], Philippe Moireau[2] , Andrew Blaber[1], Dominique Chapelle[2]

[1] Simon Fraser University, Vancouver, Canada
[2] Inria, Palaiseau, France

Abstract

Seismocardiography (SCG) is measurement of sternal acceleration caused by heart beats. Although fiducial cardiac events have been associated with seismocardiogram extrema, the forces that cause the vibrations are unknown. The goal of this study was to create a 3D model of the thorax capable of modelling its vibrations under heart-like forces.

We used the standard equations for damped elastic wave propagation. The mechanical properties of sternal and costal bone, as well as costal cartilage and lung tissue were identified. Displacement was fixed at 0 *where the ribs reached the spine, a force was input where the heart was in direct contact with the thorax. The simulation was run on a life-like volume mesh.*

A zone of observation was identified on the xiphoid process, where normal displacement was averaged. This average was considered to simulate seismocardiograms and exhibited clear fiducial point analogs that were detectable automatically.

In the next steps, we will couple the thoracic deformation model to a 3D beating heart model, incorporating contact boundary conditions that take into account the pericardium. Ultimately, we will create a thoracic model capable of returning seismocardiogram signals to enable solving inverse problems, and patient-specific modelling.

1. Introduction

Seismocardiography (SCG) records low-frequency (<0.25 Hz) sternum vibrations caused by the beating of the heart [1,2]. Recent developments in MEMS accelerometer technology have rekindled research interest in the technique [3,4].

Such devices have been used to accurately obtain heartbeat intervals [5–7], and the possibility of using SCG to obtain useful heart rate variability indices has been explored [7–9]. One of the main limitations of all these algorithms is the differences in the signal between individuals. While the fiducial points are almost always identifiable in a healthy signal, their relative amplitudes as well as the behaviour of the complete signal can be quite variable.

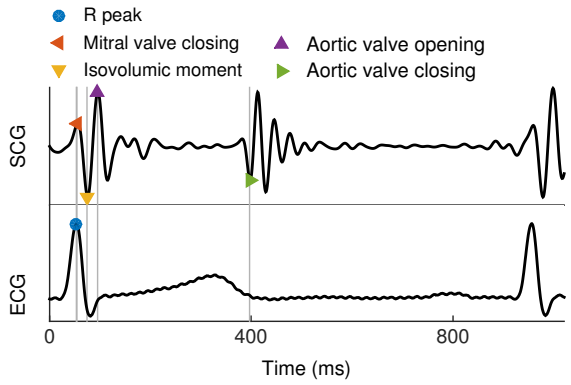

Figure 1: Example electrocardiogram (ECG) and seismocardiogram (SCG) with relevant fiducial points.

The timing of peaks observed in SCG have been related to significant cardiac events, the main ones being mitral valve closing (MC), isovolumic moment (IM) and aortic valve opening (AO) during the systolic cycle, and aortic valve closure (AC) during the diastolic cycle (Fig. 1). The assignment of these fiducial points was based on the echocardiogram analysis of SCG morphology [10, 11]. Precise mechanical timings of the cardiovascular system that can only be obtained from SCG depend critically on accurately identified fiducial points [12, 13].

Although we have identified on the SCG the moments when some important cardiac events occur, we remain largely ignorant of the forces that cause them. Indeed, in the case of the aortic valve opening and closing fiducial points, it is implausible that the low frequency vibration peaks are caused by the valves themselves. In the case of the isovolumic moment fiducial point, the exact meaning of the timing is highly implicit. The definition of this point is the absolute minimum attained by the signal during isovolumic contraction, and isovolumic contraction itself is defined as the entire lapse of time between mitral valve closure and aortic valve opening. So far, then, the IM point has a clear significance only on SCG, with an imprecise physiological interpretation.

The goal of this study was to design a 3D representation

of the thorax to simulate SCG and explore the precise mechanical causes of sternum vibrations during heart beats.

Important initial work has been conducted on a SCG heart and rib model [14]. This earlier model included practical simplifications that rendered the derived results difficult to interpret. To strengthen the physiological interpretation of the results, we performed simulations on a life-like 3D model of the thoracic cage. This model incorporated measured values for the viscoelastic properties of cortical bone, cancellous bone, and costal cartilage.

To simulate the SCG measurement, a force function representing a heart beat was applied on the zone of contact between the heart and the rib cage, and the acceleration of a second zone in the middle of the xiphoid process was then computed.

2. Methods

2.1. Numerical considerations

To examine the mechanical propagation of thoracic vibrations due the forces from the heart, the standard equations for damped elastic wave propagation were considered, which depend on the viscoelastic properties of the constituent materials. Small displacements and small deformations were assumed: the stress tensor σ depended linearly on the strain tensor ε, itself assumed to depend linearly on displacement gradient; and the domain of the elastic body could be identified to the initial configuration Ω. A viscous damping formulation was used, and all materials were considered isotropic.

The equation then became, for all positions $x \in \Omega$ and all time $t > 0$

$$\rho \frac{\partial^2 u}{\partial t^2} - \text{div } \big[\mathbf{C}\varepsilon(u)\big] + \text{div } \big[c_k \mathbf{C}\varepsilon\big(\frac{\partial u}{\partial t}\big)\big] = 0,$$

where $u(x,t)$ was displacement, the variable for which the system was solved , $\rho(x)$ was density, $c_k(x)$ was the stiffness-proportional damping coefficient, $\mathbf{C}(x)$ was the elasticity tensor of the given materials and $\varepsilon(u) = \frac{1}{2}(\nabla u + \nabla u^{\mathrm{T}})$ was the strain tensor. The system is considered at rest at the initial state, i.e.

$$u(x,0) = 0 \qquad \frac{\partial u}{\partial t}(x,0) = 0 \qquad x \in \Omega.$$

2.2. Viscoelastic properties of materials

The thoracic cage was considered comprise three materials: cortical bone, cancellous bone, and cartilage. The domain Ω was accordingly divided into three parts $\Omega_{\{1,2,3\}}$, where the material-dependent parameters $\rho(x)$, $c_k(x)$, and $\mathbf{C}(x)$ were constant.

The viscoelastic properties of the sternum, costal cartilage, ribs, and lungs were obtained from the literature [15–21] (Table 1). These values in the sternum and ribs were assumed to be closer to those of the iliac crest than of load-bearing bones such as the femur.

Table 1: Viscoelastic properties of the sternum, costal cartilage, and ribs.

	Cortical bone	Cancellous bone	Cartilage	Lungs
E	3.8	3.0	$5.2 \cdot 10^{-3}$	$1.0 \cdot 10^{-4}$
ν	0.3	0.3	0.3	0.4
ρ	$2.0 \cdot 10^3$	$2.0 \cdot 10^3$	$1.5 \cdot 10^3$	280
c_k	$6.7 \cdot 10^{-2}$	$6.7 \cdot 10^{-2}$	0.13	$\sim$

Young's modulus E in GPa , Poisson ratio ν, density ρ in kg/m^3 and damping parameter c_k in s.

The lung material was considered sufficiently soft (small Young's modulus), and light (low density) to be approximated with an unconstrained boundary condition on the bones and cartilage.

2.3. Boundary conditions

Three relevant boundaries $\Gamma_{\{a,b,c\}}$ were identified. Γ_a represented the area where the ribs attach to the vertebral column. The displacement there was fixed at 0 (Dirichlet boundary condition).

$$u(x,t) = 0 \qquad x \in \Gamma_a,\ t > 0. \tag{1}$$

The area of contact with the heart was represented by Γ_b, where a force F was applied uniformly. The displacement there depended on F as

$$\mathbf{C}\varepsilon(u)(x,t)\vec{n} = F(t) \qquad x \in \Gamma_b,\ t > 0, \tag{2}$$

The function F represented the force exerted on this zone by the heart. Certain assumptions on the heart and pericardium were made for the design of the force F. It was assumed that the distance between the heart and parietal pericardium was negligible in the zone Γ_b where the lungs aren't interposed between the heart and the thoracic cage (we assumed perfect contact). It was further assumed that the pericardial fluid acts as a perfect lubricant between the heart and the surrounding media, and that F was positive when the heart either pushed or rested on the thoracic cage, and was 0 otherwise. These assumptions give rise to the fact that any positive F should be applied on Γ_b in the normal direction.

$$F(x,t) = -f(t)n \qquad x \in \Gamma_b \tag{3}$$

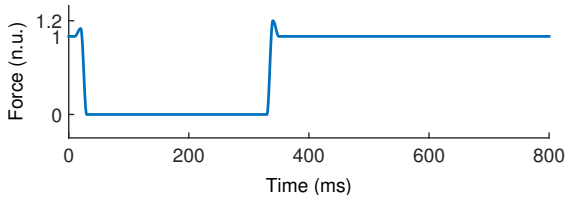

Figure 2: The force input on the thoracic zone of contact with the heart.

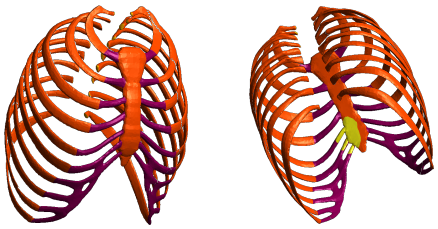

Figure 3: The volumic meshe, showing the zone of contact with the heart in yellow.

The force $f(t)$ was defined as shown in Fig. 2, and was composed mainly of a large sustained relative pull, lasting 300 ms that represented systole. This pull was flanked on both sides by smaller pushes. The first push represented atrial contraction and the second, diastolic recoil. The transition periods between the pushes and the pull were all of 10 ms.

The boundaries not included in either the area where the ribs attach to the vertebral column, or the zone of contact with the heart were represented by Γ_c

$$\Gamma_c = \Gamma/(\Gamma_a \cup \Gamma_b), \tag{4}$$

on which we assumed unconstrained displacement, which corresponds to free surface boundary conditions

$$\mathbf{C}\varepsilon(u)(x,t)\vec{n} = 0 \qquad x \in \Gamma_c,\ t > 0. \tag{5}$$

2.4. Meshes

The solution algorithm was run on a 3D life-like volume meshes. The mesh was adapted from a ZygoteBody (Zygote Media Group Inc., American Fork, UT, USA) full-body human male mesh. The sternum, costal cartilage, and ribs were considered (Fig. 3). The different parts of the initial mesh were adjusted from quadrilaterals to triangles, and then joined with 3-Matic (Materialise, Leuven, Belgium). The resulting surface mesh was automatically adjusted for regularity with Yams (Inria, France), and used to create a 3D tetrahedral mesh with GSH3D (Inria, France).

The zone of contact with the heart was identified from a standard anatomy textbook [22] (Fig. 3).

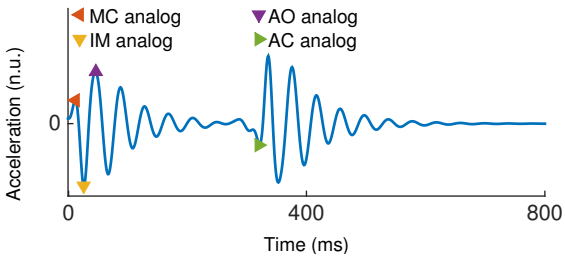

Figure 4: Simulated seismocardiogram showing four fiducial point analogs.

The solution to the system was approximated by linear finite elements with a second order centered implicit time discretization based on the Leap-Frog scheme [23].

3. Results and discussion

The goal of this study was to reproduce an SCG-like output from a physiologically correct *in-silico* 3D mechanical model of the thorax. From u, the mean acceleration was computed as

$$\bar{a} = \int_{x \in O} \frac{\partial^2 u}{\partial t^2} \cdot \vec{n}$$

where O was the zone of observation in the middle of the xiphoid process shown in Fig. 3. This acceleration was considered to simulate SCG. The overall morphology of the simulated SCG (Fig. 4) bore striking resemblance to the set of 2 wave trains seen in *in-vivo* SCG (Fig. 1).

To quantify the degree to which the simulated SCG resembled *in-vivo* SCG, it was input in an automatic annotation algorithm. The systolic segment of the simulated SCG included analogs to all three fiducial points, namely the MC, IM, and AO points. The validity of the AC point analog is less clear, as it is not the absolute minimum of the diastolic segment.

Following the main peaks, the simulated SCG exhibited oscillatory behaviour at what seems to be the first resonance frequency of the thorax. Although the physiological interpretation of this result should be approached cautiously, it encourages the notion that *in-vivo* fiducial points are caused by sudden heart movements, followed by periods of regular damped oscillations of ≈ 29 Hz.

The model considered in some detail the ribs, costal cartilage, xiphoid process, as well as the cortical and trabecular constituents of the manubrium and sternum body. For the sake of simplicity, a number of organs and physiological processes were omitted, including breathing, which is known to affect the SCG amplitude [24]. Since, however, breathing has not been shown to affect the frequency content of SCG in the relevant range, it was assumed that the system could adequately represented the end of expiration. The lungs were also not included under the assumption that

they should at most dampen the longitudinal propagation of the vibrations, especially at the end of expiration..

The most obvious missing organ is, of course, the heart itself. The mechanical modelling of a beating heart [25, 26], including its attachments at the level of the atria and the boundary conditions caused by the pericardium, is quite complex from a mathematical and numerical point of view. Its inclusion will be the next step in our modelling process. It will greatly increase the level of complexity of the model as well as its physiological relevance.

The ultimate goal is to characterize the transfer function between the movements of the heart and the derived simulated SCG, and therefore enable accelerometer measurements to return information about subject-specific heart forces and movements.

References

[1] Baevsky RM, Egorov AD, Kazarian LA. The Method of Seismocardiography. Kardiologiia, 1964.

[2] Salerno D, Zanetti JM, Poliac L, Crow R, Hannan P, Wang K, Goldenberg I, Van Tassel R. Exercise Seismocardiography for Detection of Coronary Artery Disease. American Journal of Noninvasive Cardiology, 1992.

[3] Zanetti JM, Tavakolian K. Seismocardiography: Past , Present and Future. In IEEE EMBC, 2013.

[4] Inan O, Migeotte PF, Park KS, Etemadi M, Tavakolian K, Casanella R, Zanetti J, Tank J, Funtova I, Prisk K, Di Rienzo M. Ballistocardiography and Seismocardiography: A Review of Recent Advances. IEEE Journal of Biomedical and Health Informatics, 2014.

[5] Di Rienzo M, Vaini E, Bruno B, Castiglioni P, Lombardi P, Parati G, Lombardi C, Meriggi P, Rizzo F. Wearable Seismocardiography: Towards the beat-to-beat assessment of cardiac mechanics during sleep in microgravity. ESGCO, 2014.

[6] Di Rienzo M, Vaini E, Castiglioni P, Lombardi P, Meriggi P, Rizzo F. A Textile-Based Wearable System for the Prolonged Assessment of Cardiac Mechanics in Daily Life. In IEEE EMBC, 2014.

[7] Ramos-Castro J, Moreno J, Miranda-Vidal H, García-González Ma, Fernández-Chimeno M, Rodas G, Capdevila L. Heart rate variability analysis using a seismocardiogram signal. In IEEE EMBC, 2012.

[8] Laurin A, Blaber A, Tavakolian K. Seismocardiograms return valid heart rate variability indices. In Computing in Cardiology Conference, 2013.

[9] Tadi M, Lehtonen E, Koivisto T, Paukkunen M, Paasio A, Teras M. Seismocardiography : Toward Heart Rate Variability (HRV) Estimation. In IEEE International Symposium on Medical Measurements and Applications, 2015.

[10] Crow R, Hannan P, Jacobs D, Hedquist L, Salerno D. Relationship between seismocardiogram and echocardiogram for events in the cardiac cycle. American journal of Noninvasive Cardiology, 1994.

[11] Tavakolian K, Blaber AP, Ngai B, Kaminska B, Science E, Columbia B, Physiology B. Estimation of Hemodynamic Parameters from Seismocardiogram. In Computing in Cardiology, 2010.

[12] Tavakolian K, Dumont GA, Houlton G, Blaber AP. Precordial vibrations provide noninvasive detection of early-stage hemorrhage. Journal of Shock, 2013.

[13] Salerno DM, Zanetti J. Seismocardiography for monitoring changes in left ventricular function during ischemia. CHEST Journal, 1991.

[14] Gurev V, Tavakolian K, Constantino J, Kaminska B, Blaber AP, Trayanova NA. Mechanisms underlying isovolumic contraction and ejection peaks in seismocardiogram morphology. Journal of medical and biological engineering, 2012.

[15] Cowin SC. Bone mechanics handbook, 2001.

[16] Kuhn JL, Goldstein SA, Choi R, London M, Feldkamp LA, Matthews LS. Comparison of the trabecular and cortical tissue moduli from human iliac crests. Journal of Orthopaedic Research November, 1989.

[17] Lau A, Oyen ML, Kent RW, Murakami D, Torigaki T. Indentation stiffness of aging human costal cartilage. Acta Biomaterialia, 2008.

[18] Lai-Fook SJ, Wilson TA, Hyatt RE, Rodarte JR. Elastic constants of inflated lobes of dog lungs. Journal of Applied Physiology, 1976.

[19] Lee GC, Frankus A. Elasticity properties of lung parenchyma derived from experimental distortion data. Biophysical Journal, 1975.

[20] Tawhai MH, Nash MP, Lin CL, Hoffman EA. Supine and prone differences in regional lung density and pleural pressure gradients in the human lung with constant shape. Journal of Applied Physiology, 2009.

[21] Garner E, Lakes R, Lee T, Swan C, Brand R. Viscoelastic dissipation in compact bone: implications for stress-induced fluid flow in bone. Journal of biomechanical engineering, 2000.

[22] Netter FH. Atlas of human anatomy, 2014.

[23] Joly P. Variational methods for time-dependent wave propagation problems. In Topics in computational wave propagation, 2003.

[24] Pandia K, Inan OT, Kovacs GT, Giovangrandi L. Extracting respiratory information from seismocardiogram signals acquired on the chest using a miniature accelerometer. Physiological measurement, 2012.

[25] Sainte-Marie J, Chapelle D, Cimrman R, Sorine, M. Modeling and estimation of the cardiac electromechanical activity. Computers & Structures, 2010.

[26] Chapelle D, Le Tallec P, Moireau P, Sorine M. International Journal for Multiscale Computational Engineering, 2012

Address for correspondence:

Alexandre Laurin
Department of Biomedical Physiology & Kinesiology
Simon Fraser University
8888 University Dr, Burnaby, BC V5A 1S6, Canada
laurin@sfu.ca